

Experimental, numerical, and theoretical studies of x radiation and radiative thermal conductivity in a dense laser plasma with multicharged ions

I. N. Burdonskii, V. V. Gavrilov, A. Yu. Gol'tsov, E. V. Zhuzhukalo, N. G. Koval'skii, V. N. Kondrashov, and M. I. Pergament

Troitsk Institute of Innovative and Thermonuclear Research, Troitsk 142092 Moscow Region, Russia

B. N. Bazylev, G. S. Romanov, A. N. Smetannikov, and V. I. Tolkach

Thermal- and Mass-Exchange Institute, 220072 Minsk, Belarus

M. O. Koshevoi, A. A. Rupasov, and A. S. Shikanov

P. N. Lebedev Physical Institute of the Russian Academy of Sciences, 117942 Moscow, Russia

(Submitted 25 March 1994)

Zh. Eksp. Teor. Fiz. **106**, 1628–1648 (December, 1994)

Studies have been carried out of the x radiation and radiative thermal conductivity of a plasma with multicharged ions produced by irradiating planar targets of various configurations with the focused beam from a neodymium laser over an intensity range 10^{13} – 10^{14} W/cm². The experimentally measured x-ray parameters in the spectral range 10–100 Å and their time dependence as functions of the thickness and diameter of copper targets have been compared with the results of calculations using a specially developed radiative hydrodynamics code.

Analysis of the numerical and experimental data confirms that the radiative thermal conductivity makes a substantial contribution to the energy transport process in the dense regions of the plasma corona with $n_e > 10^{21}$ cm⁻³ and that a re-emission zone develops at the surface of targets made of elements with intermediate atomic number ($Z > 20$). Techniques are proposed for diagnosing the dense regions of the plasma, based on measuring the refraction and absorption of x-ray probe radiation. © 1994 American Institute of Physics.

1. INTRODUCTION

Dense high-temperature plasmas with multicharged ions have attracted increasing attention from researchers in recent years. The possibility of creating a plasma with density close to that of solids, 10^{19} – 10^{24} cm⁻³, at temperatures in the range 10–10³ eV by irradiating targets of various materials with high-power laser beams or high-current pulsed charged-particle beams affords the opportunity in the laboratory to directly model astrophysical phenomena, study the state and properties of material under extreme conditions, and develop unique sources of x radiation, including lasers operating in the x-ray region of the spectrum and in the vacuum ultraviolet. The prospects opening up for using such sources for diagnostic purposes in biology, materials processing, and microelectronics are very alluring.

Investigations of dense high-temperature plasma are of the utmost importance for inertial confinement fusion (the initiation of thermonuclear reaction in targets with deuterium–tritium fuel by means of laser beams, beams of light or heavy ions, or linear systems). In the nonstationary and nonequilibrium plasma with which we have as a rule to deal in these studies, the dominant role is played by the processes by which energy is converted and transported. In addition to electron thermal conductivity, in a plasma with elements from intermediate to high values of the atomic number radiative thermal transport plays an important and in some cases even dominant role. The study of the generation

of x radiation and of radiative transport has acquired a special urgency in connection with the development of schemes for indirect irradiation of thermonuclear targets (the preliminary conversion of the energy of pulsed laser beams into quasiequilibrium x radiation in a plasma made of heavy elements).^{1–3} Although fairly extensive experimental material has already been accumulated on the conversion efficiency under various conditions when targets of different construction made of many materials are irradiated^{4–11} (these citations constitute only a small part of the work on this problem), a number of fundamental questions demand more detailed investigation. In Ref. 11, for example, in connection with processes that take place when laser radiation interacts with the target, attention was directed at the important role in the generation and transport of x radiation in the plasma region (the so-called re-emission zone) located between the region where the laser radiation is absorbed and the ablative surface of the target. In this zone with a relatively cold ($T_e \sim 10$ – 50 eV) and dense ($n_e \sim 10^{22}$ cm⁻³) plasma conditions arise for efficient absorption of x radiation from the more tenuous regions of the plasma corona and the subsequent re-emission of this energy in the relatively long-wavelength (tens of Ångströms) region of the spectrum with a distribution close to that of black-body radiation.

The high information content of x radiation offers considerable prospects for measuring plasma parameters and studying the processes that take place in it. However, extract-

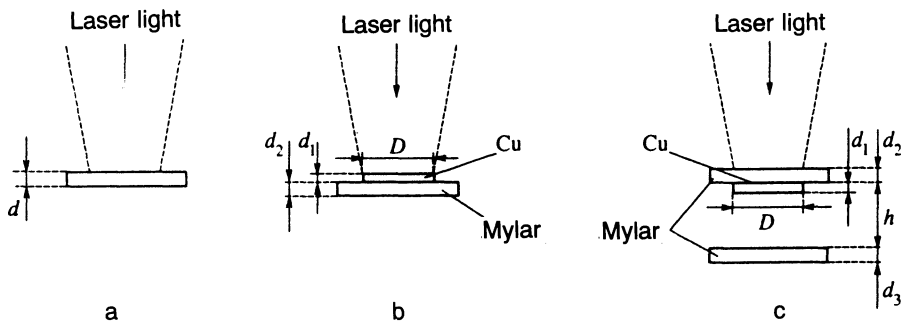


FIG. 1. Structure of targets illuminated by laser pulses in the Mishen' facility: a) single-layer target of various materials with thickness $d=1-20 \mu\text{m}$; b) two-layer target ($d_1=0.025-0.8 \mu\text{m}$ is the thickness of the copper layer of diameter D deposited on a mylar film of thickness $d_2=2-20 \mu\text{m}$); c) two-stage target (the separation between the mylar films is $h=50-250 \mu\text{m}$); $d_1=0.025-0.8 \mu\text{m}$, $d_2=2 \mu\text{m}$, $d_3=2-10 \mu\text{m}$.

ing information about the plasma parameters (temperature, density, and ionization state) in experiments with targets made of materials of relatively high atomic number ($Z > 20$) is exceedingly difficult. This is because many techniques developed over the years for diagnostics in plasmas consisting of light ions (see, e.g., Ref. 12) are based on x-ray spectral measurements of the emission from relatively simple H-, He-, and Li-like ions (as a rule, such ionization states result when targets of, e.g., Mg, Al, Si are irradiated). These techniques are naturally inapplicable when targets of heavier elements with multielectron ions structures are irradiated. The technique of active x-ray illumination of the plasma is also complicated, in particular, due to the strong absorption of the probe radiation. Consequently, the development of techniques for diagnosing plasmas consisting of ions of relatively high atomic number is a problem of importance in its own right. In particular, the above remarks about the re-emission zone suggest that spectral-time analysis of soft x-radiation from the plasma would enable one to obtain information about the formation and evolution of this zone.

Note also that there are great difficulties arising in connection with simulation of the processes of x-ray generation and radiative transport in a dense plasma with a complex ion composition. Since the thermodynamic parameters and the optical properties (the emission and absorption coefficients) of the plasma are strongly dependent on the distribution function of the ions with respect to ionization and excitation states, a fairly complicated and detailed physical model is necessary for adequate calculations of the plasma evolution. Under these conditions the need for experimental investigations is obvious. Reliable experimental data not only permit the justification for the assumptions used in the model to be verified, but also enable one to obtain additional information about atomic constants. On the other hand, the difficulty of direct measurements necessitates a method of investigation based on combining the results of numerical calculations of some complexity with the results of specially formulated experiments.

2. EXPERIMENTAL DESIGN AND PROCEDURE

The experiments were carried out in the "Mishen" (Russian for "target") facility, a detailed description of which was given in Ref. 13. The neodymium phosphate glass laser system of the Mishen' device produces two beams with the following parameters.

Main beam: wavelength $1.054 \mu\text{m}$, pulse length $\sim 2 \text{ ns}$, total energy $100-200 \text{ J}$; beam divergence $2 \cdot 10^{-4} \text{ rad}$; energy contrast $> 10^6$.

Diagnostic beam: pulse length $\sim 0.3 \text{ ns}$, total energy $10-20 \text{ J}$ at wavelength $1.054 \mu\text{m}$, and $5-10 \text{ J}$ at wavelength $0.53 \mu\text{m}$; beam divergence 10^{-4} rad .

The diagnostic complex of the Mishen' device includes apparatus for controlling the laser radiation parameters in each experiment and a broad selection of devices intended for obtaining information about the parameters and behavior of the resulting plasma by optical and x-ray techniques.¹⁴ Pinhole cameras with absorbent filters, spectrographs with plane and convex crystals (quartz, mica, CsAP, KAP), vacuum x-ray diodes in combination with various absorbing filters and multilayer mirrors, and an automated measurement system based on absolutely calibrated thermocouple calorimeters are used to record and analyze the x radiation from the plasma.¹⁵ A spectrograph with transmitting diffracting grating $1 \times 0.1 \text{ mm}^2$ made of gold (period $1 \mu\text{m}$; ratio of gap width to period $1/3$) in combination with an x-ray image-converter camera was used to measure the x-ray emission of the plasma in the range $10-100 \text{ \AA}$ with a resolution of 20 ps and a spectral resolution of $\sim 3 \text{ \AA}$ (Ref. 16). For time-integrated spatially resolved x-ray spectral measurements we used a tungsten transmitting diffraction grating with period $1 \mu\text{m}$ on a round patch (aperture) of diameter $25 \mu\text{m}$.

Targets of various designs were illuminated in the vacuum chamber. Depending on the problems encountered in specific experiments, and in order to create optimum conditions for producing and measuring plasma with appropriate parameters, both the properties of the laser radiation and the illumination conditions were varied (diameter of the focal spot, light intensity, uniformity of the intensity distribution within the focal spot, shape of the laser pulse), as well as the design and material of the target. We irradiated planar massive targets and foils of various thickness made of Al, Cu, mylar, as well as multilayer and multiple (two or more thin foils separated at some distance from one another in the direction of propagation of the laser beam). Schematics of the targets used in the experiments are displayed in Fig. 1.

3. THEORETICAL MODEL AND CODES USED IN THE NUMERICAL CALCULATIONS

In support of the experimental studies we developed a one-dimensional radiative-gasdynamics code to model the

interaction between an intense flux of laser radiation (with power density 10^{12} – 10^{14} W/cm² and nanosecond pulse length) and solid targets (including multiple targets) made of various materials. The laser radiation is absorbed due to inverse bremsstrahlung in the plasma which is expanding into vacuum. Energy is transported in the plasma by means of electron thermal conductivity and radiative heat transfer. At the leading edge of the thermal wave a shock wave develops, propagating through the cold material toward the rear surface of the target. As the mass of the heated material and its temperature increase the process of gasdynamic expansion of the plasma and radiative cooling begin to play the major role in the redistribution of the energy.

This model presupposes separate temperatures for the electron and ion components of the plasma; energy is transported by electron thermal conductivity and the intrinsic nonequilibrium radiation of the plasma, maintaining local thermodynamic equilibrium in the electron and ion components. Accordingly the equations of radiative gasdynamics in the two-temperature approximation in Lagrangian coordinates take the following form:

$$\begin{aligned}
 u &= \frac{\partial x}{\partial t}, \quad \frac{1}{\rho} = \frac{\partial x}{\partial m}, \quad \frac{\partial u}{\partial m} + \frac{\partial p}{\partial m} = 0, \\
 \frac{\partial \varepsilon_T}{\partial t} + p \frac{\partial(1/\rho)}{\partial t} + \frac{1}{\rho} \operatorname{div}(S + W_e) &= Q, \\
 \frac{\partial \varepsilon_i}{\partial t} + p_i \frac{\partial(1/\rho)}{\partial t} &= (T_e - T_i)/\tau_{ei}, \\
 \varepsilon_T &= \varepsilon_e' + \varepsilon_i, \quad \varepsilon_e = \varepsilon_e' - Q_i, \quad p = p_e + p_i.
 \end{aligned} \tag{1}$$

Here u is velocity, ρ is density, p is pressure, m is the mass coordinate, ε_T is the specific internal energy of the plasma, S is the power density of the laser radiation, W_e is the thermal flux density due to the electron thermal conductivity, Q is a source term representing the contribution of the laser energy, and Q_i is the ionization energy T is temperature. The subscripts e and i refer to electron and ion components respectively.

To determine the radiation field we use the time-dependent radiative transfer equation in the multigroup approximation.¹⁷ The entire spectral range is divided into N spectral groups, taking into account the properties of the spectrum which are characteristic of a particular target material (e.g., the presence of line radiation):

$$\begin{aligned}
 \frac{1}{c} \frac{\partial F_j^\pm}{\partial t} + \frac{\partial(C_j^\pm F_j^\pm)}{\partial x} &= J_j - k_j^p \eta_j^\pm F_j^\pm, \\
 S &= 2 \sum_{j=1}^N (C_j^- F_j^- + C_j^+ F_j^+).
 \end{aligned} \tag{2}$$

Here F_j^\pm are the average one-sided fluxes in the j th spectral group, k_j^p is the average Planck absorption coefficient in the group, J_j is the source function in the j th spectral group [in the approximation of local thermodynamic equilibrium (LTE), $J_j = k_j^p B_j$, where B_j is the Planck function], and C_j^\pm are the averages over the j th group of the one-sided cosines in the hemispheres.

The initial and boundary conditions are as follows:

$$\begin{aligned}
 t=0: \quad T &= T_0, \quad \rho = \rho_0(m), \quad p = p_0, \quad u = 0; \\
 m=0: \quad F^+ &= 0, \quad W_e = 0, \quad p = 0; \\
 m=M: \quad F_j &= 0, \quad W_e = 0, \quad p = 0.
 \end{aligned} \tag{3}$$

To solve the gasdynamic equations we use a completely conservative scheme with artificial viscosity, while for the radiative transport equations we use an implicit difference scheme which permits an arbitrary number of discontinuities in temperature and the optical properties of the medium.¹⁸ The heat transfer process is calculated implicitly by means of tridiagonal inversion.

An important step is obtaining the thermodynamic, transport, and optical properties of the material by solving the equations of state over a broad range of densities (from solid to plasma), taking into account phase transitions, and over a broad range of temperatures. For copper and aluminum we use semiempirical equations of state,¹⁹ describing the properties of the material from the compressed solid state with the transition to liquid and then into liquid-vapor and then to vapor (plasma). In the plasma region we used the Saha system of equations with corrections for nonideal behavior. We used the Barnes equation to describe the condensed phase of mylar.²⁰ All necessary information about the individual properties of the ions is found from quantum mechanical calculations using a self-consistent Hartree–Fock–Slater model.^{21,22} We included in the absorption coefficients the processes of inverse bremsstrahlung and photoionization with the optical and internal shells. The optical constants used in this study are obtained by the method of a simple neutralizing in the spectral group limits. (The number of the group for calculation was 250.)

However, the use of plasma optical and physical properties obtained in the local thermodynamic equilibrium approximation can exaggerate the x-ray yield, since the source function in the transport equation can differ considerably from the equilibrium Planck function. The reason for this is that the occupation of the emitting levels will differ substantially from the Boltzmann value: excited states can be populated less than under LTE conditions. In that case we use the collisional-radiative model to calculate the ionization state of the plasma and its thermophysical and optical properties. In this model the populations of the ion states are found by solving a system of kinetic equations:²³

$$\frac{dN_m}{dt} = \sum_{n=1}^M K_{mn} N_n, \tag{4}$$

$$\frac{dN_z}{dt} = \sum_{n=1}^M K_{zn} N_n, \tag{5}$$

where z is the ground state of the ions. Here the coefficients K_{mn} determine the rates of the collisional and radiative processes. In many cases we can restrict ourselves to the solution of the time-independent equations, in which the right-hand side reduces to zero:

$$\sum_{n=1}^M K_{mn}N_n = 0, \quad (m \neq n). \quad (6)$$

In solving Eqs. (4), (5), and (6) we include the following processes: electron excitation and deexcitation of ions, impact ionization and three-body recombination, spontaneous emission of excited ions, and also photo- and dielectronic recombination.²⁴ In view of the great complexity of this system we usually restrict ourselves to a small number of states in the ion, and the rates of the processes are calculated using simple empirical formulas. These are the Mieve formula for impact excitation, the Lotz formula for impact ionization, the Kramers formula for photorecombination, and the Burgess formula for dielectronic recombination.

In the present work we use the approximation of time-independent kinetics (5) for determining the ionization composition and thermophysical properties of the plasma, employing more accurate reaction rates than those cited above. For collisional processes the Born and Born-Coulomb approximations are used.²⁴ For calculating the rates of the photoprocesses the tabulated values of their cross sections were used, which (like the other atomic properties) were found from self-consistent calculations of the Hartree-Fock-Slater equations using the technique described in Refs. 23 and 24. The dielectronic recombination rates were found from detailed balance of the emission and autoionization processes. It is also important to note that for elements with *d* and *f* electrons the process of resonance ionization²⁵ can play an important role, as follows: an interior *p*-electron from the state $3p^63d^{n+1}$ is excited into the state $3p^53d^{n+1}$ with subsequent autoionization $3p^53d^{n+1} \rightarrow 3p^63d^{n-1} + e$. Under certain conditions the rate of this process is a factor of ten greater than the rate of the direct ionization process. We also assumed that the self-field of the radiation does not affect the population of the states. Of course, this assumption imposes certain limitations on the applicability of the model.

By solving the system of equations (5), taking into account the processes listed above, we find the ionization state of the plasma, its thermophysical properties, and the absorption and emission coefficients. Note that the emission coefficients in this case will be smaller than under LTE conditions. It should also be noted that for the interior electrons the absorption and emission coefficients cannot be related by the balance condition through the Planck function, since the unbalanced autoionization process arises for them. In this connection the difference in absorption and emission will be substantial in the short-wavelength region of the spectrum.

4. EXPERIMENTAL AND CALCULATED RESULTS: DISCUSSION

As revealed by studies carried out previously,⁸⁻¹⁰ the x-ray yield has a complicated dependence on the atomic number of the target material and is characterized by three local maxima for $Z = 10 - 13$, $25 - 40$, and $60 - 70$. The occurrence of these maxima is essentially due to the different efficiencies with which line radiation is generated by multi-charged ions. The location of the maxima depends primarily on the power density of the laser radiation at the target sur-

face, which determines the temperature of the resulting plasma. Hence the maximum conversion efficiency of the plasma is found to be considerably higher as the atomic number increases.

For laser illumination of targets with intermediate and large atomic numbers the energy of the x-ray emission from the plasma amounts to tens of percent of the applied energy. After carrying out preliminary experiments we determined that under our experimental conditions one of the largest conversion efficiencies was achieved when copper was used as the target material. Intense line radiation from copper ions is mainly concentrated in the narrow spectral range $10 - 13 \text{ \AA}$, while line radiation from ions with large atomic numbers is distributed over a broad range of wavelengths, which is found to be undesirable in a number of cases and interferes with application of diagnostic techniques. Subsequent experiments were carried out with copper targets, whose construction was described above. Spectral selection made it possible to obtain information about the tenuous hot plasma corona by detecting short-wavelength line radiation, while analysis of the long-wavelength radiation provided information about processes in the denser and colder regions of the plasma.

Before discussing these results, let us say something more about calculating the conversion efficiency using experimental data obtained primarily with the four-channel calorimetric system. To cut off the radiation in the visible and far-ultraviolet range these detectors were covered with thin filters (e.g., one of the calorimeters had an aluminum foil of thickness 3.2 \mu m). Naturally, the calorimeters detect only a part of the total number of photons incident on a filter. In the case of a copper target the main contribution to the useful signal comes from line radiation photons with a wavelength of $10 - 13 \text{ \AA}$, not only because of the high intensity of this radiation but also because the filters have high transmissivity in this spectral range. The transmissivity of the filter integrated over time and wavelength (in the range $1 - 100 \text{ \AA}$) depends not only on the time-varying plasma temperature but also on the target thickness, which, as shown above, has a substantial effect on the nature of the spectral and temporal distribution of radiation intensity. The transmission also depends on the position of the detector, since the spectral distributions of the intensity in the front and rear hemispheres may differ due to absorption in the unvaporized part of the target. The values of the transmission coefficients of the filters were calculated using the codes described above, which simulate the x-ray emission from the laser plasma and were used to process the experimental data.

The experimental data on the dependence of the re-emission conversion efficiency into the forward hemisphere (i.e., in the direction opposite the laser beam) on the thickness of the copper slab (Fig. 2) under the specified conditions of illumination shows that there is a critical value $d_{cr} \approx 0.2 \text{ \mu m}$ for this thickness. For targets of thickness above the critical value the radiative losses of the plasma do not increase substantially (other conditions being equal). The values of d_{cr} are approximately the same for all target diameters used. This behavior of the conversion efficiency as a function of target thickness is also predicted by the numerical model

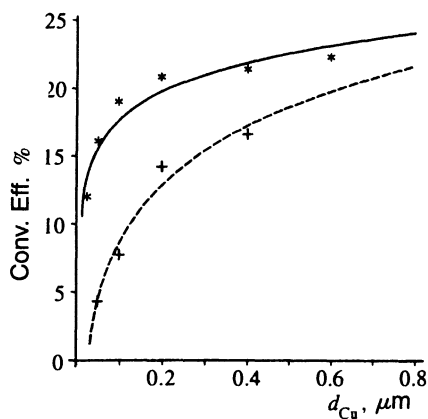


FIG. 2. Conversion efficiency of the re-emission into the front hemisphere as a function of the thickness of a copper layer of diameter $300 \mu\text{m}$ on a mylar substrate ($I = 5 \cdot 10^{13} \text{ W/cm}^2$): *—experimental data; +—results of calculations.

(Fig. 2); the discrepancy in magnitude between the experimental and calculated results can be explained by the one-dimensional nature of the code. The magnitude of d_{cr} in fact also characterizes the depth of the “burn-through” of the copper target, or, in other words, the mass of copper ablated from the illuminated surface of the target during the course of the laser pulse and entering into the plasma corona. Under our illumination conditions ($I \sim 5 \cdot 10^{13} \text{ W/cm}^2$) the rate of burn-through, as shown by the calculations, is of order $0.1 \mu\text{m/ns}$ for copper and $1 \mu\text{m/ns}$ for mylar. If the thickness of the copper target is increased above d_{cr} the conversion efficiency remains essentially unchanged, since the additional mass of material passes into the corona only after the action of the heating pulse terminates and cannot reach a high temperature. For a copper target of thickness $0.05 \mu\text{m}$ all of the copper is heated to high temperature as early as $\sim 0.5 \text{ ns}$ following the onset of illumination, the ablation wave has reached the mylar substrate, and oxygen, carbon, and hydrogen ions begin to enter the corona. Since the effective charge of the plasma ions is thereby decreased in comparison with the case of a plasma consisting entirely of copper ions, the x-ray intensity drops markedly.

Experimental data obtained for a copper target of fixed thickness reveal that the x-ray yield (into the hemisphere facing the laser beam) depends on both the energy in the laser pulse and on the geometrical dimensions of the target (Fig. 3). For example, for a target of diameter 3 mm the conversion efficiency is found to be approximately twice as high as in the case of a target of diameter $300 \mu\text{m}$. In our opinion, this increase in the x-ray conversion efficiency is explained by the influx of material from the peripheral regions of the target, which are negligibly heated by the refracted laser radiation and the x radiation of the plasma corona. Other conditions being equal, increasing the thickness of the mylar substrate to $20 \mu\text{m}$ causes the conversion efficiency to decrease by $10-15\%$.

Returning to Fig. 2, we ascertain that for a copper target of thickness and diameter $0.2 \mu\text{m}$ and $300 \mu\text{m}$ respectively the conversion efficiency for x radiation into the rear hemi-

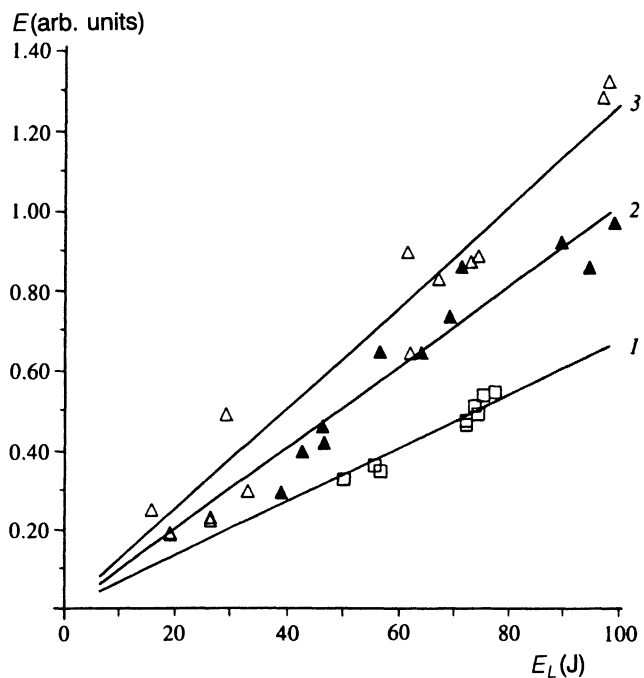


FIG. 3. Experimental x-ray energy yield as a function of the energy of the laser pulse for a copper layer of thickness $0.1 \mu\text{m}$ with different diameters on a mylar substrate: 1 (\square) $D_{\text{Cu}} = 300 \mu\text{m}$; 2 (\blacktriangle) $D_{\text{Cu}} = 500 \mu\text{m}$; 3 (\triangle) $D_{\text{Cu}} = 3 \text{ mm}$.

sphere amounts to $20-25\%$ (the diameter of the focal spot is equal to $\sim 250 \mu\text{m}$). When the target diameter increases to 3 mm the conversion efficiency attains the value of $40-50\%$. (Note that this value of the conversion efficiency is quite high, but by no means a world record: according to Mead *et al.*,⁴ approximately 80% of the laser energy was converted into x-ray emission of the plasma when a gold target was illuminated.) These data were obtained assuming an isotropic distribution of the intensity of x-ray emission from the plasma, which is quite reasonable at least for thin targets. At such high conversion efficiencies the x radiation begins to play an important role in the physical processes that occur when the high-power laser pulse interacts with the target. Thus, whereas in the early stages of illumination ($< 0.3 \text{ ns}$ after the onset of the laser pulse) the principal energy transport mechanism is electron thermal conductivity, subsequently, as shown by the results of the calculations, the contribution of radiative transfer becomes very important. The unvaporized (rear) part of the target under these conditions is subject to the action of an intense flux of x radiation with power density $5 \cdot 10^{12} - 10^{13} \text{ W/cm}^2$ and can heat up to higher temperatures (in comparison with the heating due to the shock wave). This is confirmed by experimental data which we obtained²⁶ when two- and three-layer targets (mylar-aluminum and copper-mylar-aluminum, with the radiation coming from the direction of the mylar and the copper respectively). The conclusion that the aluminum is heated to high temperature in these experiments is based on the observation of time-resolved line radiation from H- and He-like ions of this material. When two-layer targets were irradiated

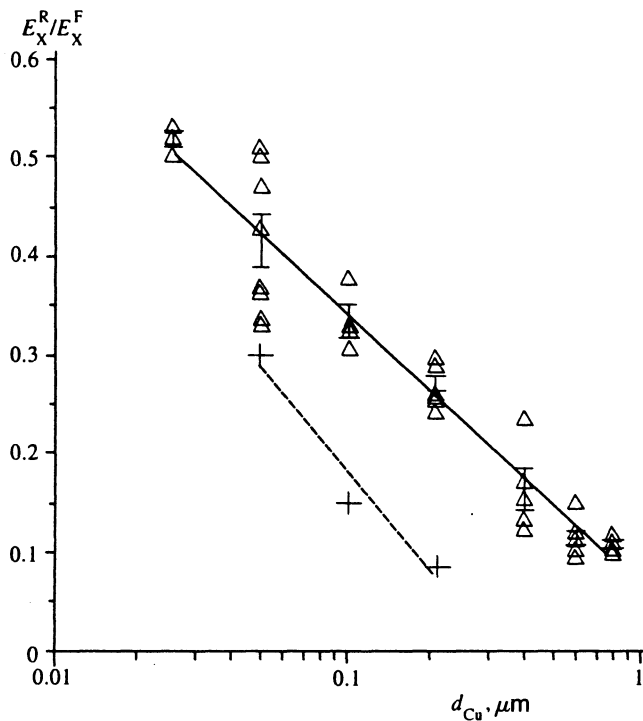


FIG. 4. Ratio of the x-ray energy yield in the backward direction (E_X^R) to that in the forward (E_X^F) hemisphere as a function of the thickness of a copper layer of diameter $300 \mu\text{m}$ on a mylar substrate [$I = (3-5) \cdot 10^{13} \text{ W/cm}^2$]; Δ —experimental data; $+$ —results of calculations.

the line radiation was detected beginning ~ 1 ns after the start of the laser pulse, i.e., with a delay to allow the rear part of the target to be heated by the thermal wave and the aluminum to then enter the hot plasma corona. Adding an additional copper layer of thickness $\sim 1 \mu\text{m}$ to the mylar (which increased the intensity of the x-ray emission by a factor of several dozen) caused the line radiation from the aluminum ions to be detected immediately after the start of illumination, that is, the flux of x-ray photons from the corona heated up the back part of the target to high temperature practically instantaneously.

The transport of the x radiation in the target can be characterized by the dependence of the ratio of the signal from calorimeters positioned alongside and in front of the target (i.e., the intensity of the radiation into the rear and front hemispheres) as a function of the thickness of the copper layer for a target diameter of $300 \mu\text{m}$ (Fig. 4). These experimental data are in satisfactory agreement with the results of the calculations. For a copper layer of thickness $0.025 \mu\text{m}$ approximately half as many x-ray photons are emitted into the rear hemisphere as in the direction of the laser beam. The total conversion efficiency in this case is equal to 15–17%.

The totality of experimental and numerical results described above can be explained fairly well by using the concept of a re-emission zone formed near the surface of the illuminated target. Next we discuss experiments whose immediate purpose was to obtain information about the formation and evolution of this zone.

The spectral distribution of the intensity of soft x radia-

tion from a laser plasma was studied in the wavelength range $10-100 \text{ \AA}$ with high temporal resolution. The principal apparatus used was the spectrograph based on the transmission diffraction grating described above, together with an x-ray image converter camera. As is well known, when radiation is recorded with a spectrograph using a transmission diffraction grating the radiation spectra in different diffraction orders are superposed, which makes it necessary to perform nontrivial mathematical processing of the data in order to recover the actual spectral distribution of the intensity.¹⁶

We will say a few words about the results of experiments in which copper layers of different thickness were subjected to radiation. The results obtained by processing the data from the spectrograph with transmission diffraction grating are shown in Fig. 5, which demonstrates the time evolution of the spectral distribution of plasma radiation for copper layers of thickness $0.05, 0.2,$ and $0.4 \mu\text{m}$ (the target diameter was $300 \mu\text{m}$).

The difference in the time development of the spectral intensity in the wavelength range $40-70 \text{ \AA}$ for targets with deposited layers of different thickness is noteworthy: 1 ns after the start of the pulse in this spectral range targets with a layer of thickness $0.2 \mu\text{m}$ and above show an increase in the intensity compared with the case when the layer thickness was equal to $0.05 \mu\text{m}$. At later times this increase becomes very pronounced. In the short-wavelength part of the spectrum ($10-13 \text{ \AA}$) no such effects are observed.

Based on our previous remarks concerning the formation of a re-emission zone we can conclude that the spectral distribution measured with a copper layer of thickness $0.05 \mu\text{m}$ characterizes the emission primarily from the hot plasma corona, whereas the behavior of the spectrum in the long-wavelength region for a copper layer of thickness $0.2 \mu\text{m}$ and above reflects the formation of a re-emission zone. In fact, as shown by the calculations, the increase in radiation intensity in the range $40-70 \text{ \AA}$ for the case of a relatively thick target (see Fig. 6, in which the calculated radiation spectra are shown for two thicknesses of copper at a particular time) is due to the emission from copper ions in a low ionization state (CuXI–CuXVI) specifically from this region. Within it there is a sharp rise in the temperature from tens to several hundreds of eV on the characteristic spatial scale $5-10 \mu\text{m}$ and a drop in density from solid values to $\sim 10^{-3} \text{ g/cm}^3$. The optical depth of this zone for radiation with wavelength $40-70 \text{ \AA}$ is of order unity. The results of our calculations show that the energy supplied to this zone by the radiative mechanism is comparable with the contribution from electron thermal conductivity. As shown by the above experimental data, the time of formation for the re-emission zone under our conditions amounts to 1–1.5 ns. For a copper layer of thickness $0.025-0.1 \mu\text{m}$ and target diameter approximately equal to the diameter of the focal spot, the formation of this region is hindered by a shortage of material with high Z , responsible for efficient conversion. Specifically, for laser radiation of power density $5 \cdot 10^{13} \text{ W/cm}^2$ the rate at which target material is ablated in our experiments is equal to $\sim 10^{-7} \text{ g/ns}$ (Ref. 27) and all the material of a copper layer of thickness, e.g., $0.05 \mu\text{m}$ goes into the corona and is heated to a temperature of order 0.5 keV in a time of

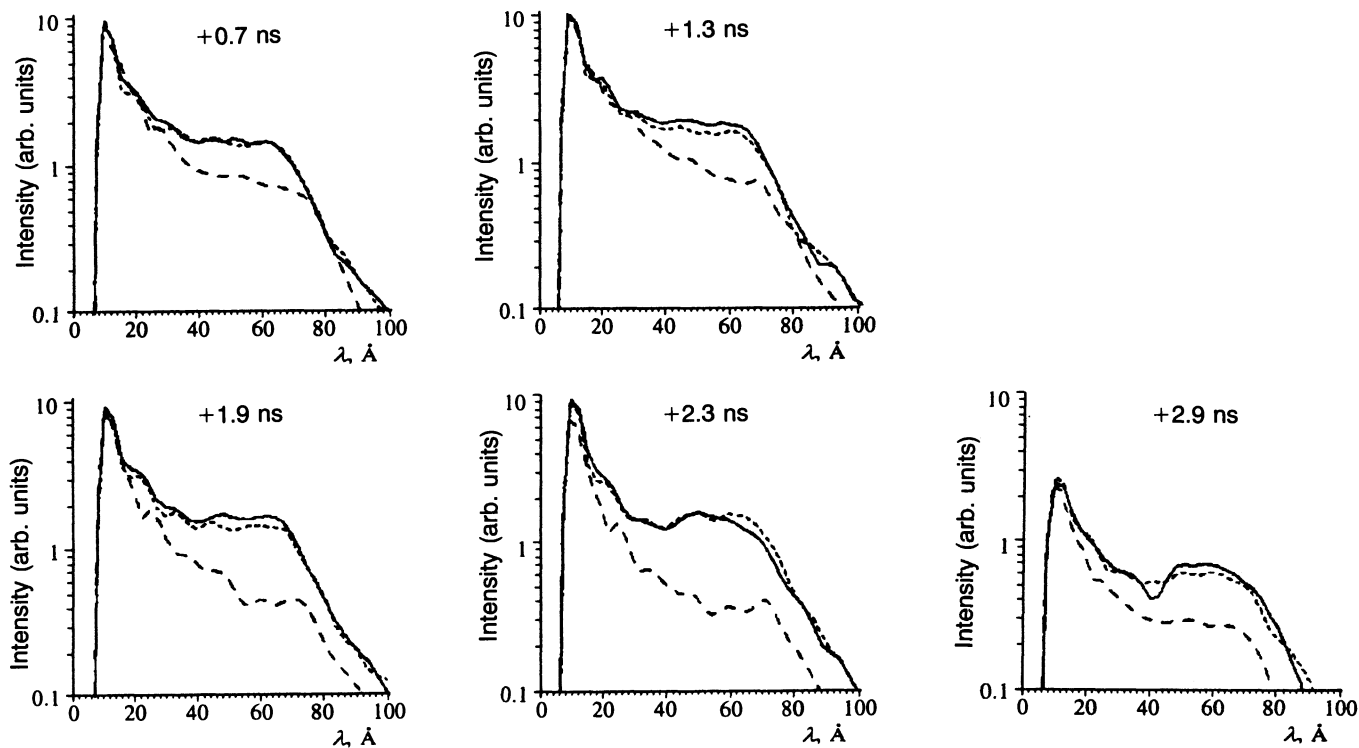


FIG. 5. Spectral intensity of the x radiation from a plasma at various times after the start of illumination of targets with copper layers of thickness $0.05 \mu\text{m}$ (dashed trace), $0.2 \mu\text{m}$ (dotted trace), and $0.4 \mu\text{m}$ (solid trace); $I = 5 \cdot 10^{13} \text{ W/cm}^2$.

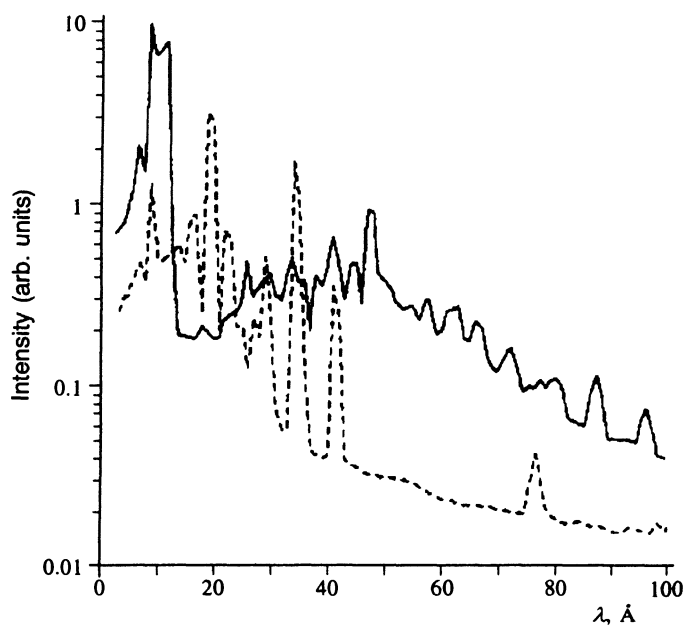


FIG. 6. Calculated spectra of the x radiation from the plasma 1.3 ns after the start of illumination of a target with copper layers of thickness $0.05 \mu\text{m}$ (---) and $0.2 \mu\text{m}$ (—); $I = 5 \cdot 10^{13} \text{ W/cm}^2$.

0.2–0.3 ns after the start of illumination. The ablated material of the substrate does not take part in the formation of the re-emission zone, in view of the low absorptivity of oxygen, carbon, and hydrogen ions in the x-ray region of the spectrum.

In our experiments, as noted above, in addition to the thickness of the copper layer we also varied the diameter. Figure 7 shows the evolution of the x-ray spectral distribution in the plasma for layer diameters of 300 and 500 μm (layer thickness 0.1 μm). Increasing the target diameter is also seen to increase the radiation intensity in the spectral range 40–70 Å at times 1–1.5 ns after the start of the laser pulse. The observed rise in intensity can be explained as the emission of the relatively cold plasma formed outside the focal spot and the influx of this plasma into the central parts of the plasma corona mentioned above, which increases the mass of material and is equivalent to increasing the initial thickness of the copper layer. The formation of the peripheral plasma was noted in Ref. 27. Thus, we can conclude that two-dimensional effects have a strong influence on the efficiency with which x radiation is generated by a laser-plasma source.

As seen from the results given above, the direct measurement of radiation parameters in the wavelength range 50–150 Å is fruitful from the standpoint of obtaining information about the energy transport process in the dense regions of targets with intermediate and high values of Z . In essence, under certain conditions in targets with relatively large values of Z , the mechanism for converting laser radi-

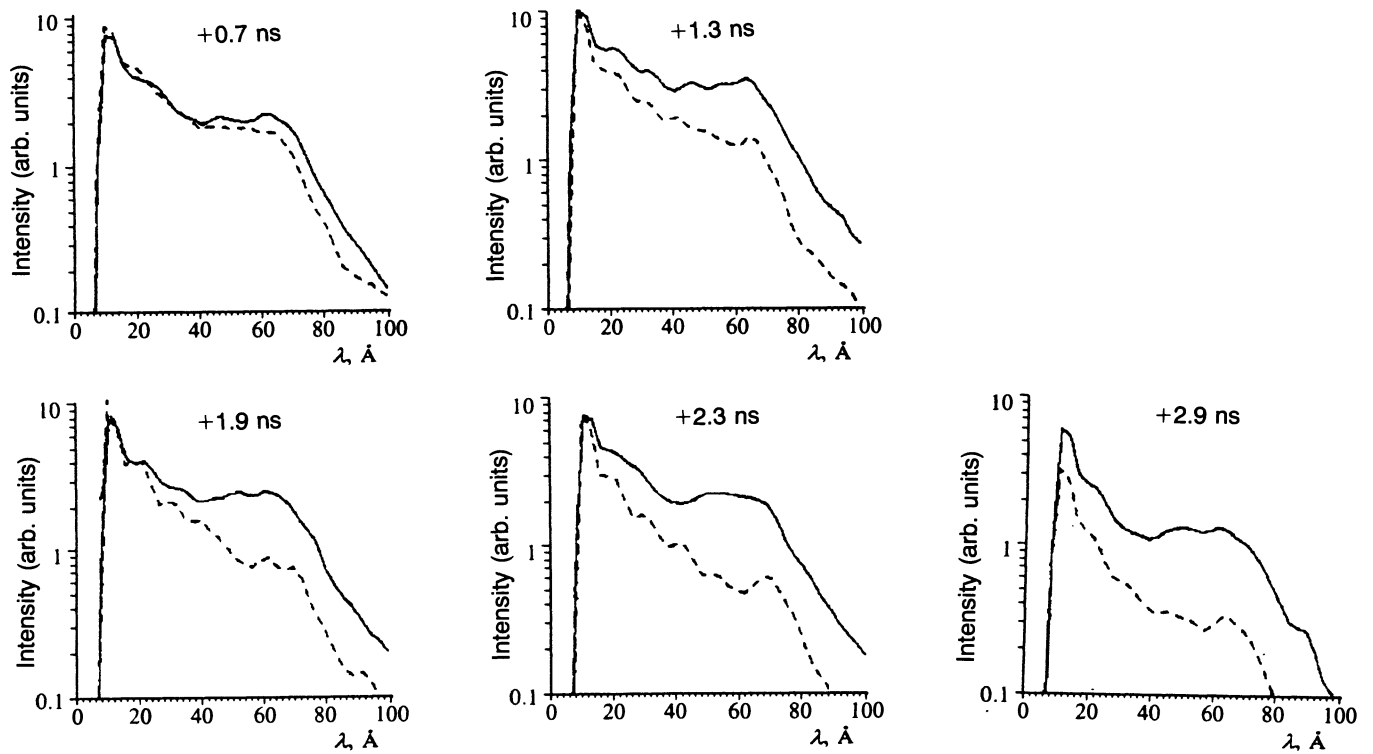


FIG. 7. Spectral intensity of the x radiation at different times following the start of illumination of targets with copper layers of thickness $0.1 \mu\text{m}$ and diameter $300 \mu\text{m}$ (dashed trace) and $500 \mu\text{m}$ (solid trace); $I = 5 \cdot 10^{13} \text{ W/cm}^2$.

tion into x rays undergoes a wholesale change. What this means is that processes in which photons are absorbed and repeatedly emitted begin to play a more and more important role. Under our conditions, as shown by the experimental data and the results of the numerical calculations, this process begins to be manifested in the spectral range $40 - 70 \text{ \AA}$. It is clear that increasing the temperature, just like increasing the total mass of the plasma, should broaden the spectral region in which the emission processes begin to dominate. It seems to us that more detailed analysis of the energy balance and dynamics of "soft" spectra will enable one to develop an understanding of the physical processes and techniques for increasing efficiency which may be applicable also in the case of re-emission layers of higher temperature and at shorter wavelengths of the re-emitted x radiation.

One possible technique is to control the conversion efficiency by varying the target parameters and illumination conditions. The general direction of the program outlined in Ref. 28 is to find a situation when the optical thickness in some spectral region is of order unity by making the target parameters and illumination conditions consistent with one another. As shown in Ref. 28, this can be achieved if we use elements with large values of Z and reduced density as targets. The technology for fabricating targets of materials such as gold, copper, etc., with densities in the range $0.01 - 1 \text{ g/cm}^3$ was developed jointly in the Institute of Inorganic Chemistry and the Lebedev Institute. Experiments on the illumination of such targets are currently only in the planning stage.

In our experiments we have studied another possibility, associated with the use of multistage targets. Multistage targets consist of one or several thin (several microns) mylar films separated from one another by a few tens to a few hundreds of microns. A layer of material with high Z of thickness in the range $0.01 - 1 \mu\text{m}$ is applied to the inner side of one (or both) foils.

Examples of the experimental results obtained by illuminating multiple targets are shown in Fig. 8. Note the typical features of the resulting x-ray spectra. The most important is that when multiple targets with a copper layer on the rear surface of the illuminated foil of thickness $\sim 0.1 \mu\text{m}$ are irradiated, a noticeable increase (by almost a factor of two) in the x-ray yield is observed in the spectral range $50 - 100 \text{ \AA}$, an effect that occurs in the late stage of illumination at a time $\sim 1.8 \text{ ns}$ after the start of the laser pulse. Increasing the thickness of the copper layer to 0.3 or more microns does not produce a corresponding increase in the yield in this spectral range.

Comparison of spectra recorded in experiments in which multiple targets with copper layers of thickness $\sim 0.1 \mu\text{m}$ on the rear surface of the mylar film are irradiated with different values of the interfoil gap (including the case when the target in the second stage is absent entirely) reveals that the increase in the yield is greatest for gaps of order $100 \mu\text{m}$. The increase in the yield may be related to the conversion of laser radiation into x rays in the copper plasma of reduced density that fills the interfoil gap when the copper layer is unloaded from the rear surface of the first stage of the target. The time

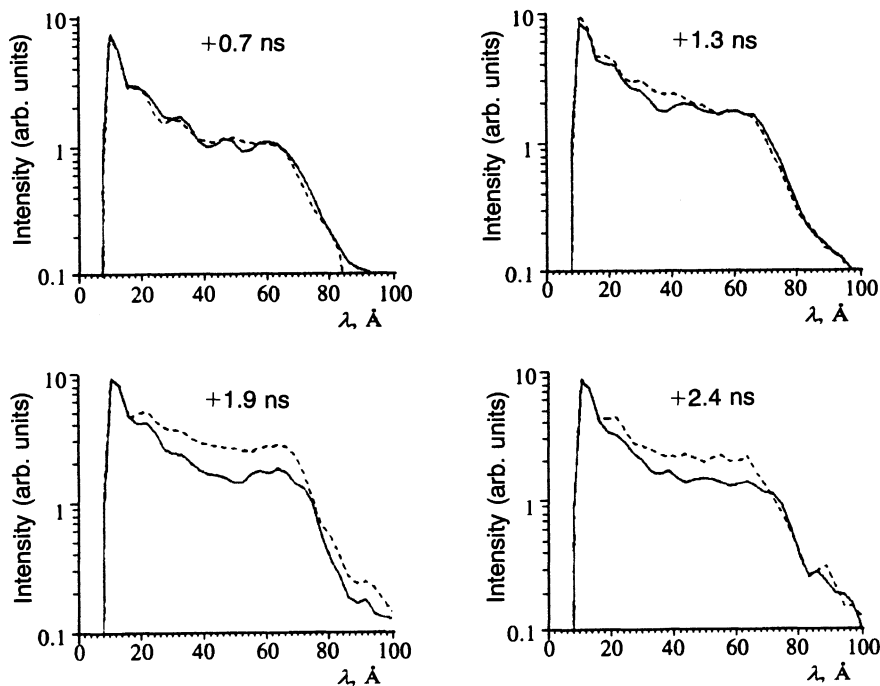


FIG. 8. Spectral intensity of the x radiation from a plasma at different times following the start of illumination of a target with a copper layer of thickness $0.2 \mu\text{m}$ and diameter $300 \mu\text{m}$ on the back side of a mylar film of thickness $1 \mu\text{m}$ (solid trace) and of the same target when a second mylar film of thickness $3 \mu\text{m}$ (dashed trace) is located $120 \mu\text{m}$ behind it; $I = 5 \cdot 10^{13} \text{ W/cm}^2$.

delay in this case should be determined by the typical speed of material in the unloading wave and the value of the interstage gap. The dependence of the yield on the size of the gap between the stages and also the fact that the effect is small when the copper layer on the rear surface is thick can be explained on the basis of the ideas described above.

Although the proposed model unquestionably needs further experimental and numerical verification, our data imply that by proper choice of the multistage target parameters it is possible to effectively change the size of the conversion coefficient in the x-ray wavelength range $50 - 100 \text{ \AA}$. At the present time we are planning to carry out experiments with two-stage targets of this type in which the first-stage target undergoes preliminary irradiation with a low-power (of order $10^{10} - 10^{11} \text{ W/cm}^2$) auxiliary laser beam. This would enable us to vary the thickness of a layer of material with high Z and the size of the energy input to the target independently in the experiments, thereby extending the possibilities for experimental simulation of physical processes.

We now pause to discuss the development of direct methods for diagnosing physical processes in the dense regions of high- Z targets. The data thus obtained are useful in the design of such experiments.

Most importantly, satisfactory agreement between experimental and numerical data on x-ray emission give reason to hope that the calculated profiles of plasma parameters (we are mainly interested in the dense region of the plasma) correspond in some measure to actual parameter profiles whose direct measurement we propose to carry out. Thus, in the case of a copper plasma the typical spatial scales of the density and temperature profiles obtained in the calculations for regions of the plasma with density $\sim 10^{21} \text{ cm}^3$ are of order $5 - 10 \mu\text{m}$. Magnitudes of this order are employed as initial

values for estimating the required spatial resolution of the diagnostic techniques in question.

Having in mind active x-ray diagnostic techniques, we are particularly interested in the optical parameters of the dense plasma (the absorption and emission coefficients) for heavy elements as a function of the wavelength over a wide range of electron densities and temperatures $n_e = 10^{20} - 10^{22} \text{ cm}^3$, $T_e = 10 - 500 \text{ eV}$ for the spectral range $10 - 10^4 \text{ eV}$. As an example, in Fig. 9 we plot the absorption coefficients for a lead plasma for several values of the electron density and temperature. These traces clearly distinguish the regions in which absorption occurs due to the photoeffect (short wavelengths) and the bremsstrahlung mechanism (long wavelengths). Such data are essential for analyzing the diagnostic possibilities of x-ray spectroscopy of plasmas in different spectral ranges.

Finally, spectral measurements and experiments on the illumination of targets of different elements (both time-integrated and time-resolved) enable us to optimize (from the standpoint of increasing the signal-to-noise ratio, and also that of obtaining high contrast) the choice of materials in the primary and auxiliary targets, the time at which the measurements are carried out, and also the spectral range. As an example, Fig. 10 shows the evolution of the spectral distributions of copper and lead plasmas in the range $10 - 100 \text{ \AA}$, enabling us to properly design an experiment in which the radiation passes all the way through. We have obtained similar data for targets of various materials (aluminum, carbon, copper, lead, dysprosium, etc.).

On the basis of the currently available calculated and experimental results we propose the following diagnostic techniques.

Absorptive measurements for probe radiation in the

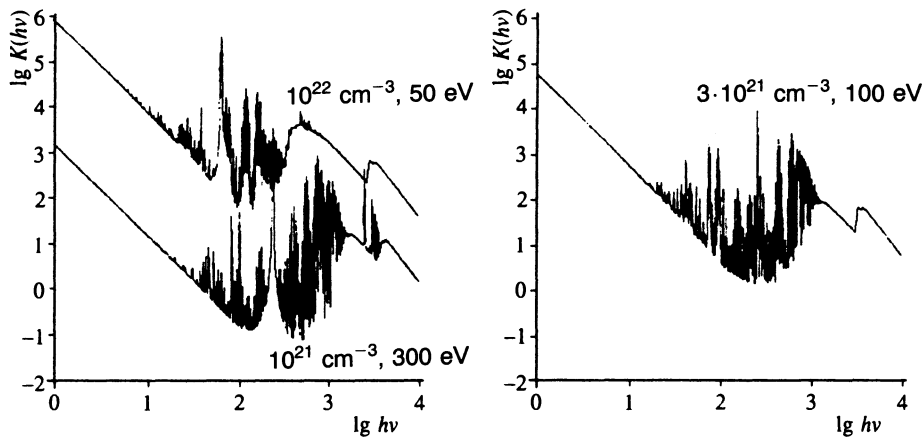


FIG. 9. Calculated values of the absorption coefficient of plasma consisting of lead ions for three values of the electron density and temperature.

range 7–12 Å. As shown by the results of calculating the absorption of a lead plasma (Fig. 9), at electron densities $\sim 10^{21}$ cm $^{-3}$ in this spectral range the optical thickness of the plasma is of order unity, which makes it possible to perform absorption measurements. Taking into account that the absorption under these conditions is due to the photoeffect, we can use the method to measure the ion density profile. We consider two possible versions of the technique. One of these, associated with the use of a point source and detection of radiation by means of a crystal spectrograph, was employed previously in experiments on the stability of thin ablatively accelerated foils, described in Ref. 29. The spatial resolution was about 25 μ m. The time resolution determined by the length of the laser pulse used to produce the diagnostic x-ray source was about 0.3 ns.

Another approach is to illuminate special targets consisting of thin (several tens of μ m) of the high-Z material in

question (lead) of diameter 250 μ m on a mylar substrate of thickness a few μ m. Copper or aluminum patches of thickness 0.1–1 μ m and dimensions 20 \times 20 μ m 2 were applied along the target diameter on the lead surface with a spatial period of 40 μ m. As an example, Fig. 11 shows a schematic of the diagnostic and a photo from a pinhole camera recorded in an experiment on the illumination of a mylar target with copper microspots inside the focal spot. In this case the spatial resolution in the direction of the density gradient—normal to the target surface—was ~ 20 μ m (in principle the resolution can be improved to ~ 5 –10 μ m). In the direction parallel to the target surface the resolution was probably determined by the dimensions of the copper patches and was equal to about 20 μ m (neglecting the transverse motion of material). The time resolution depends on the thickness of the copper in the spots.

The second technique is based on measuring the refrac-

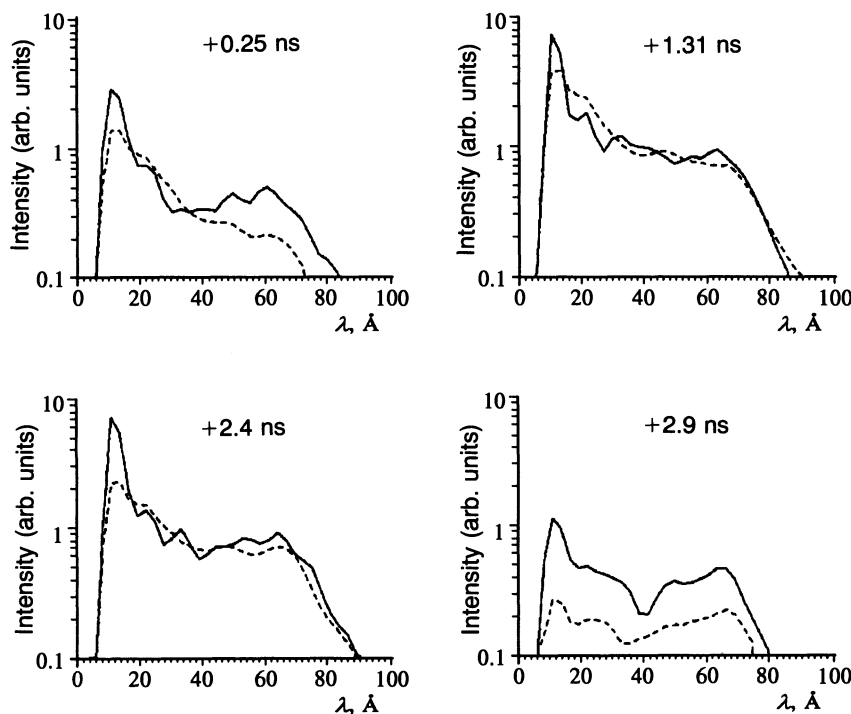


FIG. 10. Spectral intensity of the x radiation from a plasma at different times following the start of illumination of targets made of copper (solid trace) and lead (dashed trace) of thickness 20 μ m; here $I = 5 \cdot 10^{13}$ W/cm 2 .

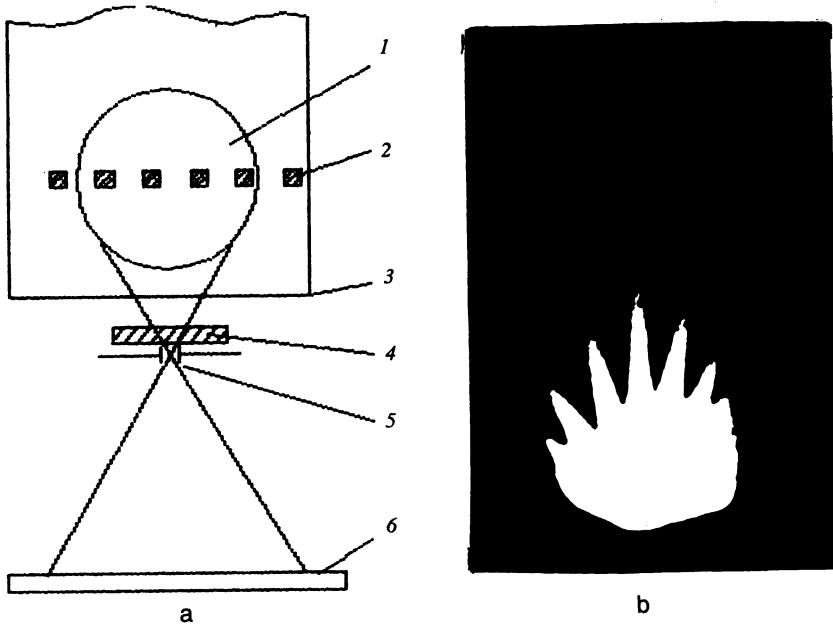


FIG. 11. Diagnostic schematic (a) and pinhole photo (b) taken in an experiment on the illumination of a mylar target with copper microspots within the focal spot ($I = 5 \cdot 10^{13} \text{ W/cm}^2$): 1) focal spot of diameter $250 \mu\text{m}$; 2) copper layers of thickness $0.2 \mu\text{m}$ deposited on an area of $20 \times 20 \mu\text{m}^2$ (the separation between adjacent patches is $40 \mu\text{m}$); 3) mylar film of thickness $10 \mu\text{m}$; 4) beryllium filter of thickness $20 \mu\text{m}$; 5) pinhole camera with hole of diameter $15 \mu\text{m}$; 6) photographic film.

tion of the probe radiation. As is well known, interference measurements of electron density, which have been carried out successfully in laser plasmas using probe beams in the visible range, are limited to densities of order 10^{21} cm^{-3} , in part by the strong refraction of the probe radiation. When soft x radiation is used to carry out refractive measurements in the dense regions of the plasma corona ($n_e > 10^{21} \text{ cm}^{-3}$) the principal difficulty is the small refraction angle. Simple numerical estimates reveal that the refraction angles under typical conditions are of order 10^{-3} rad when radiation with wavelengths in the range $70 - 130 \text{ \AA}$ is used as the probe, which is a very measurable quantity. The calculations reveal that the absorption coefficient in this spectral range undergoes abrupt changes as a function of wavelength. Furthermore, as shown by Fig. 9, within this range we can distinguish parts of the spectrum of order $3 - 5 \text{ \AA}$ in width, where the optical thickness of the plasma is small and refractive measurements can be carried out. Note that this spectral range is in some measure forced on us: at short wavelengths the effect of diffraction increases (recall that the size of the refraction angle is proportional to the square of the wavelength, whereas the diffraction grows only linearly) while at long wavelengths the absorption of the probe radiation by the plasma becomes unacceptably large. To implement the technique it is proposed to use a modification of the shadow technique, familiar as knife-edge diffraction.³⁰ The main point of this technique is the use of reflective optics in the x-ray range to create an image with high angular resolution (of order 10^{-4} rad). Such unique optical elements have become attainable in recent years and have already made it possible to achieve spatial resolution of order $1 \mu\text{m}$ in experiments on x-ray diagnostics of laser plasmas.³¹

5. CONCLUSION

We have studied the conversion of laser radiation into x radiation in a plasma formed when targets made from elements with different values of Z are illuminated with light of intensity $I = 10^{13} - 10^{14} \text{ W/cm}^2$.

For a copper target the conversion efficiency for x-ray photons in the range $0.1 - 1.5 \text{ keV}$ reaches a value of 50% at $I = 5 \cdot 10^{13} \text{ W/cm}^2$.

The conversion efficiency is observed to depend strongly on the transverse dimensions of the illuminated area (two-dimensional effects) and the thickness of the vaporized layer. Through the use of specially designed multiple targets the yield of soft x rays ($40 - 70 \text{ \AA}$) is increased approximately twofold.

The formation of a re-emission zone in the plasma corona between the region where the laser radiation is absorbed and the ablation surface has a significant effect on the yield and the spectral composition of the soft x radiation. By analyzing the x-ray spectrum in the wavelength range $10 - 100 \text{ \AA}$ obtained with high time resolution ($\sim 50 \text{ ns}$) we have shown that it is possible to study the conditions under which this zone is formed when copper targets are illuminated.

We have developed a radiative hydrodynamics code. The good agreement between the experimental data and the results of the calculations shows that the physical model on which this code is based is reasonably complete. This in turn makes it possible to obtain believable x-ray spectra from laser plasmas of complex composition.

By analyzing the experimental and numerical data we can conclude that at light intensities above 10^{13} W/cm^2 in plasmas formed at the surface of a target with relatively large values of the atomic number ($Z > 20$), the contribution of the radiative thermal transfer to energy transport processes becomes comparable with that due to the Spitzer mechanism.

Diagnostic techniques for the dense regions of the plasma corona ($10^{21} - 10^{23} \text{ cm}^{-3}$) based on measurements of refraction and absorption of a probe beam of x rays from an external laser-plasma source have been presented, supported by the calculations and the results of preliminary experiments.

We wish to thank O. L. Dedova, S. V. Il'ina, I. A. Kargin, V. M. Petryakov, and A. S. Skryabin for their assistance

in conducting the experiments and processing the results of the measurements. This work was performed with financial support from the Russian Fund for Fundamental Research.

- ¹H. Nuckols, Laser Program Annual Report UCRL-50021-81 (1982), p. 3.
- ²K. Kondo, H. Nishimura, H. Sakura *et al.*, Jpn. J. Appl. Phys. **29**, 1695 (1989).
- ³R. Sigel, R. Pakula, S. Sakabe, and G. D. Tsakiris, Phys. Rev. A **38**, 5779 (1989).
- ⁴W. C. Mead, E. K. Stover, R. L. Kauffman *et al.*, Phys. Rev. A **38**, 5275 (1988).
- ⁵H. N. Kornblum, R. L. Kauffman, and J. S. Smith, Rev. Sci. Instr. **57**, 2179 (1986).
- ⁶A. V. Vinogradov and V. N. Shlyaptsev, Kvantovaya Élektron. (Moscow) **14**, 5 (1987) [Sov. J. Quantum Electron. **11**, 1 (1987)].
- ⁷I. N. Burdovskii, V. V. Gavrilov, A. Yu. Gol'tsov *et al.*, Fiz. Plazmy **13**, 819 (1987) [Sov. J. Plasma Phys. **13**, 473 (1987)].
- ⁸P. J. Malozzi, H. M. Eppstein, R. G. Young *et al.*, J. Appl. Phys. **45**, 1891 (1974).
- ⁹T. Mochizuki, T. Yabe, K. Okada *et al.*, Phys. Rev. A **33**, 525 (1986).
- ¹⁰D. R. Kania, H. Kornbul, B. A. Hammel *et al.*, Phys. Rev. A **46**, 7853 (1992).
- ¹¹R. Sigel, K. Eidmann, F. Lavarenne, and R. Schmaltz, Phys. Fluids B **2**, 199 (1990).
- ¹²V. A. Boiko, A. V. Vinogradov, S. A. Pikuz *et al.*, X-ray spectroscopy of laser plasmas, in N. G. Basov (ed.), Radio Engineering Series, Vol. 27 [in Russian], VINITI, Moscow (1980).
- ¹³V. A. Bolotin, I. N. Burdovskii, A. Yu. Gol'tsov *et al.*, Kurchatov Atomic Energy Institute Preprint No. 5967/7 (1989).
- ¹⁴V. A. Bolotin, I. N. Burdonsky, V. V. Gavrilov *et al.*, Rev. Sci. Instrum. **61**, 3259 (1991).
- ¹⁵B. A. Bryunetkin, V. D. Gladkov, O. V. Kopistko *et al.*, Methods for Studying the Spectral and Relaxation Properties of Atoms in Ions [in Russian], NPO VNIIFTRI, Moscow (1990).
- ¹⁶V. A. Bolotin, V. V. Gavrilov, A. Yu. Gol'tsov *et al.*, Zh. Tekh. Fiz. **63** (11), 703 (1993) [Phys. Tech. Phys. **38**, 985 (1993)].
- ¹⁷B. N. Bazylev and G. S. Romanov, Inzh.-Fiz. Zh. **41**, 318 (1981).
- ¹⁸B. N. Bazylev, I. M. Kozlov, G. S. Romanov *et al.*, Heat Exchange in the Action of Radiation Fluxes on Materials [in Russian], ITMO ANB, Minsk (1990).
- ¹⁹A. V. Bushman, A. L. Ng, and V. E. Fortov, Equation of State in Extreme Conditions [in Russian], Institute of Theoretical and Applied Mechanics of the Siberian Division of the Academy of Sciences of the USSR, Novosibirsk (1981).
- ²⁰R. S. Hawke, D. E. Duerre, and J. G. Hueble, J. Appl. Phys. **43**, 3734 (1972).
- ²¹B. N. Bazylev, L. V. Golub, G. S. Romanov, and V. S. Tolkach, Inzh.-Fiz. Zh. **58**, 1012 (1990).
- ²²B. N. Bazylev, L. V. Golub, G. S. Romanov, and V. S. Tolkach, *ibid.*, **59**, 62 (1990).
- ²³V. I. Derzhiev, A. G. Zhidkov, and G. I. Yakovlenko, Study of Ions in a Nonequilibrium Dense Plasma [in Russian], [in Russian], Énergoatomizdat, Moscow (1986).
- ²⁴L. A. Vainshtein, N. I. Sobel'man, and E. D. Yukov, Excitation of Atoms and Broadening of Spectral Liner, Springer, New York (1980).
- ²⁵F. Broillard and J. W. McGowan (eds.), Physics of Ion-Ion and Electron-Ion Collisions, Plenum, New York (1983).
- ²⁶V. A. Bolotin, I. N. Burdonsky, V. V. Gavrilov *et al.*, Laser and Particle Beams **10**, 753 (1992).
- ²⁷L. A. Bol'shov, I. N. Burdonskii, A. L. Velikovich *et al.*, Zh. Eksp. Teor. Fiz. **92**, 2060 (1987) [Sov. Phys. JETP **65**, 1160 (1987)].
- ²⁸G. A. Vergunova and V. B. Rozanov, Kvantovaya Élektron. (Moscow) **19**, 263 (1992) [Sov. J. Quantum Electron. **16**, 239 (1992)].
- ²⁹V. A. Bolotin, I. N. Burdonsky, V. V. Gavrilov *et al.*, Laser and Particle Beams **10**, 685 (1992).
- ³⁰L. A. Vasil'ev, Shadowgraphy Techniques [in Russian], Nauka, Moscow (1968).
- ³¹M. Desselberg, T. Afshar-rad, F. Khaltak *et al.*, Appl. Optics **30**, 2285 (1991).

Translated by David L. Book